

1 **U-Pb dating of middle Eocene-Pliocene multiple tectonic pulses in the Alpine**  
2 **foreland**

3  
4 **Luca Smeraglia<sup>1,2,3</sup>, Nathan Looser<sup>4\*</sup>, Olivier Fabbri<sup>2</sup>, Flavien Choulet<sup>2</sup>, Marcel Guillong<sup>4</sup>,**  
5 **Stefano M. Bernasconi<sup>4</sup>**

6  
7 1. National Research Council, IGAG, Rome, Italy

8 2. Chrono-Environnement, UMR 6249, Université de Bourgogne-Franche Comté, 25000 Besançon, France

9 3. formerly at Dipartimento di Scienze della Terra, Sapienza Università di Roma, P.le Aldo Moro 5, 00185, Roma

10 4. Geological Institute, ETH Zürich, Sonneggstrasse 5, 8092 Zürich, Switzerland

11  
12 \*Corresponding author e-mail address: [Nathan.looser@erdw.ethz.ch](mailto:Nathan.looser@erdw.ethz.ch)

13  
14 **Abstract.** Foreland fold-and-thrust belts record long-lived tectono-sedimentary activity, from  
15 passive margin sedimentation, flexuring, and further involvement into wedge accretion ahead of an  
16 advancing orogen. Therefore, dating fault activity is fundamental for plate movement  
17 reconstruction, resource exploration or earthquake hazard assessment. Here, we report U-Pb ages of  
18 syntectonic calcite mineralizations from four thrusts and three tear faults sampled at the regional  
19 scale, across the Jura fold-and-thrust belt in the northwestern Alpine foreland (eastern France).

20 Three regional tectonic phases are recognized in the middle Eocene-Pliocene interval: (1) pre-  
21 orogenic faulting at  $48.4 \pm 1.5$  and  $44.7 \pm 2.6$  Ma associated to the far-field effect of the Alpine  
22 compression, (2) syn-orogenic thrusting at  $11.4 \pm 1.1$ ,  $10.6 \pm 0.5$ ,  $9.7 \pm 1.4$ ,  $9.6 \pm 0.3$ , and  $7.5 \pm 1.1$   
23 Ma associated to the formation of the Jura fold-and-thrust belt with possible in-sequence thrust  
24 propagation, and (3) syn-orogenic tear faulting at  $10.5 \pm 0.4$ ,  $9.1 \pm 6.5$ ,  $5.7 \pm 4.7$ , and at  $4.8 \pm 1.7$   
25 Ma including the reactivation of a pre-orogenic fault at  $3.9 \pm 2.9$  Ma. Previously unknown faulting  
26 events at  $48.4 \pm 1.5$  and  $44.7 \pm 2.6$  Ma predate by  $\sim 10$  Ma the reported late Eocene age for tectonic

27 activity onset in the Alpine foreland. In addition, we dated the previously inferred re-activation of  
28 pre-orogenic strike-slip faults as tear faults during Jura imbrication. The U-Pb ages [document a](#)  
29 [minimal time frame for the evolution of the Jura FTB wedge by possible in-sequence thrust](#)  
30 [imbrication above the low-friction basal décollement consisting of evaporites.](#)

31

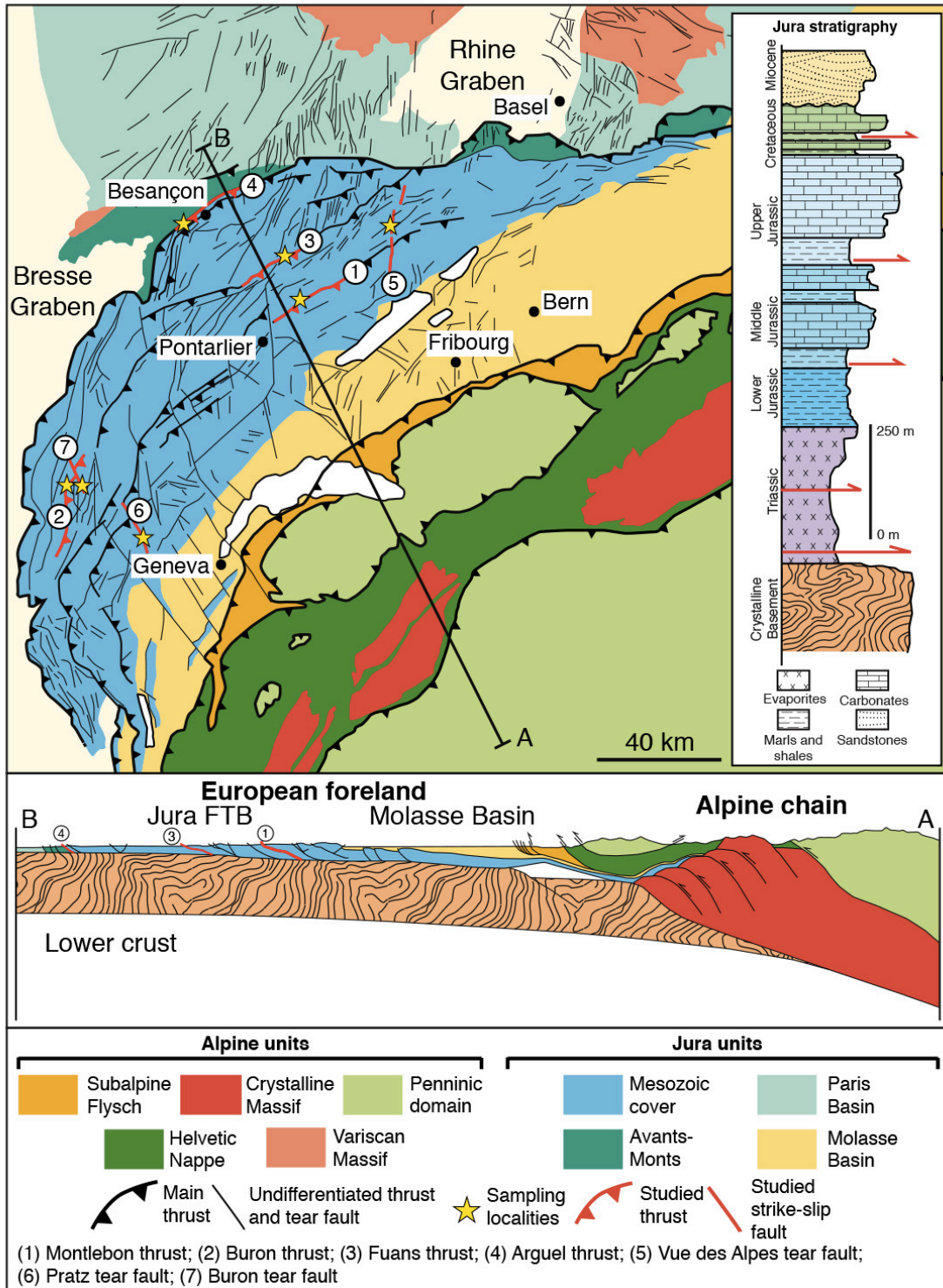
## 32 **1. Introduction**

33 Foreland fold-and-thrust belts develop at the external edges of orogens and are characterized  
34 by a multiphase tectono-sedimentary history including: pre-orogenic sedimentation, uplift at the  
35 peripheral bulge of the advancing orogen, progressively accelerating subsidence followed by syn-  
36 tectonic sedimentation, and accretion of the sedimentary cover into the foreland fold-and-thrust belt  
37 (Lacombe et al., 2007). Unraveling the timing of these tectonic events is fundamental for plate  
38 kinematic modelling, natural resource exploration, paleoseismicity, and topography evolution  
39 studies (Vergés et al., 1992; Craig and Warvakai, 2009). However, deciphering the different  
40 tectonic phases is complicated by the overprinting of inherited structures by progressively younger  
41 tectonic events.

42 This issue [is](#) addressed by dating syn-tectonic sediments and, more recently, [better](#)  
43 [constrained](#) through dating of fault activity with K-Ar,  $^{40}\text{Ar}/^{39}\text{Ar}$ , and U-Pb and [U-Th](#) methods (Van  
44 der Pluijm et al., 2009; Vrolijk et al., 2018). In particular, calcite U-Pb and [U-Th](#) geochronology  
45 (Roberts et al., 2020) is the unique method for dating syntectonic calcite mineralizations. This  
46 technique has been applied for dating single faults in extensional, strike-slip, and compressional  
47 settings (Goodfellow et al., 2017; Nuriel et al., 2017; Hansman et al., 2018; Smeraglia et al., 2019;  
48 Carminati et al., 2020). So far, the dating of multiple faults at the regional scale across a foreland  
49 fold-and-thrust belt remains rare (Beaudoin et al., 2018; Looser et al., 2021).

50 [In this study](#), we dated syntectonic calcite mineralizations from four thrusts and three tear  
51 faults sampled across the Jura fold-and-thrust belt (Jura FTB, eastern France, [Fig. 1](#)) by laser  
52 ablation inductively coupled plasma mass spectrometry (LA-ICP-MS) U-Pb dating. We

53 reconstructed [three](#) tectonic phases having occurred in the middle Eocene-Pliocene period,  
 54 documenting a long-lived polyphase tectonic history of the northwestern Alpine foreland system  
 55 along the convergent boundary between European and African plates.



56  
 57 **Figure 1.** Geological map of the northwestern Alpine foreland and surrounding areas and stratigraphic column of the  
 58 main lithological units of the Jura area. Modified from [Rime et al. \(2019\)](#).

59

## 60 **2. Tectonic setting**

61 The Jura FTB is located in the foreland of the Western Alps and formed by the ongoing  
62 continental collision of the Eurasian plate with the African plate ([Sommaruga, 1997](#); [Mosar, 1999](#);  
63 [Lacombe and Mouthereau, 2002](#); [Affolter and Gratier 2004](#); [Bellahsen et al., 2014](#)) (Fig. 1).  
64 Shortening affected the Triassic-late Miocene sedimentary succession deposited on the European  
65 passive margin above the Hercynian crystalline basement and caused brittle-ductile deformation at  
66 several levels (Fig. 1) ([Philippe et al., 1996](#); [Homberg et al., 2002](#); [Ustaszewski and Schmid, 2006](#)).  
67 The sedimentary succession starts with Triassic shales and evaporites overlain by Jurassic-  
68 Cretaceous shales, marls, and limestones (Fig. 1) ([Sommaruga et al., 2017](#)). Following a Late  
69 Cretaceous-Eocene regional unconformity, Oligocene-Miocene shallow marine to continental  
70 clastic deposits of the Molasse Basin were deposited above Cretaceous limestones (Fig. 1).

71 The post-Mesozoic tectonic history of the Jura area is assumed to have started in the middle  
72 Eocene with N-S shortening related to the far field effect of the "Pyrenean orogeny" generating  
73 strike-slip faults ([Bergerat, 1987](#)). However, no absolute ages of this tectonic phase are available.  
74 Based on structural analyses and calcite U-Pb ages, two phases of normal faulting during the Late  
75 Eocene and Oligocene in the distal parts of the Molasse Basin in northern Switzerland have been  
76 documented. Normal faulting during the Late Eocene has been related to crustal extension due to  
77 the opening of the Rhine Graben, while normal faulting during the middle Miocene has been related  
78 to crustal tilting associated to uplift of the Black Forest Highlands and subsidence of the northern  
79 part of the Molasse Basin ([Mazurek et al., 2018](#)).

80 Biostratigraphic dating of syn-orogenic deposits, geomorphological observations,  
81 interpretation of seismic reflection profiles, and syntectonic calcite U-Pb ages of fault activity in the  
82 eastern tip of Jura FTB indicate that orogenic shortening started ~14.5 Ma ago (Langhian times) at  
83 the latest ([Looser et al., 2021 and references therein](#)) and is still active ([Mosar, 1999](#); [Becker, 2000](#);  
84 [Madritsch et al., 2008](#)). Shortening was accommodated by N to NE-verging and NE-SW-striking

85 thrusts and by NW-SE to N-S trending sinistral tear faults (Sommaruga, 1997) (Fig. 1). The main  
86 décollement level of the thrust system developed along Triassic evaporites (Jordan, 1992; Pfiffner,  
87 2014; Gruber, 2017; Sommaruga et al., 2017). Therefore, there is a common agreement in  
88 considering the Jura FTB mainly as the product of thin-skinned tectonics (Sommaruga, 1997).  
89 However, thick-skinned tectonics occurred in the late stage of deformation and only in the external  
90 part (Ustaszewski and Schmid, 2006, 2007; Madritsch et al., 2008; Lacombe and Bellahsen, 2016).

91 Field cross-cutting relationships and U-Pb ages of syntectonic calcite mineralizations show  
92 that tear faults were synchronously active with thrusting and folding (Sommaruga, 1997; Looser et  
93 al., 2021) and their movement continued after thrusting. In fact, in some cases, tear faults are still  
94 seismogenic (Thouvenot et al., 1998). Several authors suggested that pre-orogenic strike-slip and  
95 normal faults were reactivated in early Pliocene, respectively as tear and transpressional faults  
96 (Madritsch et al., 2008; Homberg et al., 1997; Ustaszewski and Schmid, 2006). Overall, no direct  
97 dating of this fault re-activation has been available up to date.

98

### 99 **3. Methods**

100 The following methods were used: (1) field structural analyses and vein/slickenside sampling  
101 from four major thrusts (From SE to NW: Montlebon, Buron, Fuans, and Arguel thrusts) and three  
102 NNE-SSW tear faults (Vue des Alpes, Pratz, and Buron) moving from the internal (most deformed)  
103 to the external (less deformed) parts of the Jura FTB (Fig. 1). In particular, we measured the  
104 orientation of sampled veins and the rake of sampled slickensides in order to combine U-Pb ages  
105 from veins and slickensides with structural measurements; (2) microstructural analyses with optical  
106 microscope and cathodoluminescence to unravel different phases of calcite precipitation; (3) calcite  
107 U-Pb LA-ICP-MS dating on veins and slickensides to date fault activity. In most cases, the U-Pb  
108 analyses were performed on calcite crystals showing a homogenous color or undisturbed growth-  
109 zoning under cathodoluminescence light, indicating no open-system alteration after calcite  
110 precipitation by late fluid infiltration and/or recrystallization (Figs. S1-S3). As commonly done in

111 LA-ICP-MS U–Pb carbonate dating, no disequilibrium correction for initial  $^{234}\text{U}/^{238}\text{U}$  and  $^{230}\text{Th}$  was  
112 applied. This may cause underestimation of young (<10 Ma) samples (Roberts et al., 2020).  
113 Analytical details are described in the Supplementary Material.

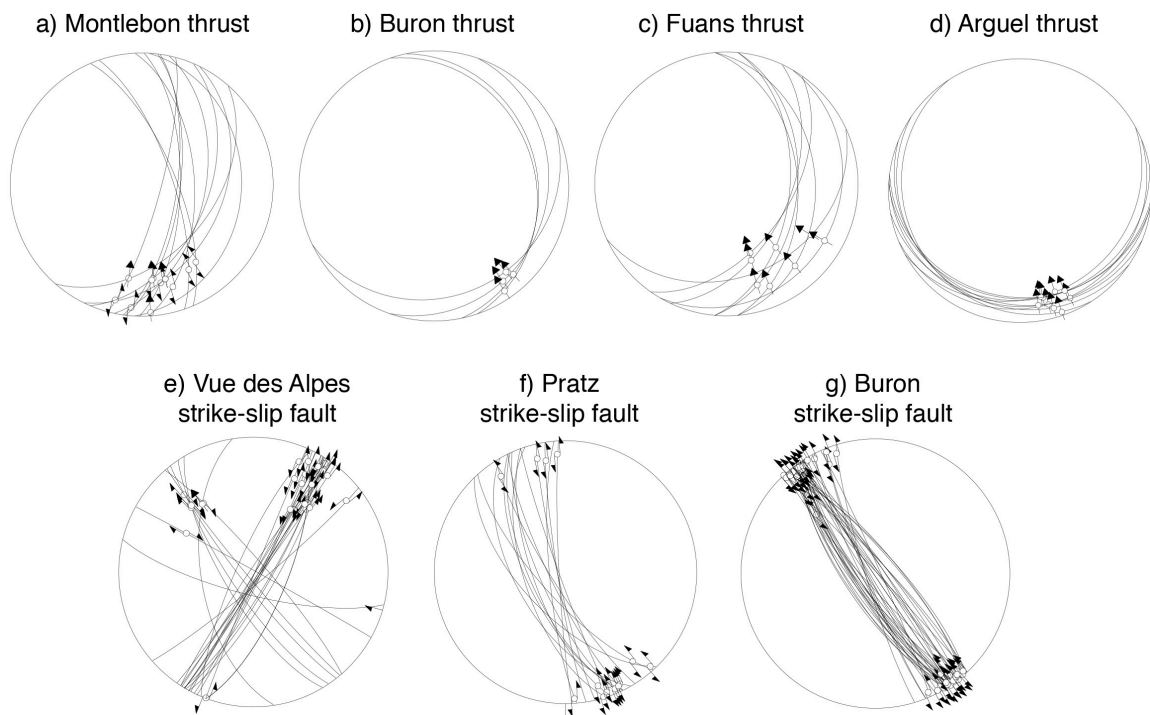
114

## 115 **4. Results**

### 116 *4.1 Structural and microstructural observations*

117 The Montlebon, Buron, Fuans, and Arguel thrusts are NNE- to SW-NE striking and N- to  
118 NW-verging thrusts (Madritsch et al., 2008; Rime et al., 2019; Smeraglia et al., 2020) (Fig. 2a-d). In  
119 particular, the Montlebon thrust is characterized by E to ESE-dipping (30-90°) thrust planes with  
120 slickenfibers showing left-lateral transpressional movements with N to NNW tectonic transport  
121 directions (Fig. 2a). The Buron thrust is characterized by E to SE-dipping (20°-30°) thrust planes  
122 with slickenfibers showing left-lateral transpressional movements with NW tectonic transport  
123 directions (Fig. 2b). The Fuans thrust is characterized by E to SE-dipping (20°-40°) thrust planes  
124 with slickenfibers showing left-lateral transpressional movements with NNW to NW tectonic  
125 transport directions (Fig. 2c). The Arguel thrust is characterized by S-dipping (10-30°) thrust planes  
126 with slickenfibers showing right-lateral transpressional movements with NNW tectonic transport  
127 directions (Fig. 2d).

128 The subvertical Vue des Alpes, Pratz, and Buron tear faults show a sinistral strike-slip  
129 displacement (Sommaruga, 1997) (Fig. 2de-g). In particular, the Vue des Alpes strike-slip fault is  
130 characterized by NE-SW-striking subvertical fault planes with slickenfibers showing sinistral  
131 movements and associated NW-SE-striking subvertical fault planes with slickenfibers showing  
132 dextral movements (Fig. 2e). Both the Pratz and Buron strike-slip faults are characterized by NE-  
133 SW-striking subvertical fault planes with slickenfibers showing sinistral movements (Fig. 2f-g).



134

135 **Figure 2.** Lower Schmidt hemisphere projection of fault-slip data and slip vectors for thrust and strike-slip faults. **(a)**

136 Montlebon thrust. **(b)** Buron thrust. **(c)** Fuans thrust. **(d)** Arguel thrust. **(e)** Vue des Alpes strike-slip fault. **(f)** Pratz

137 strike-slip fault. **(g)** Buron strike-slip fault-

138

139 Both thrusts and strike-slip faults cut through Middle-Upper Jurassic and Lower Cretaceous

140 limestones. The fault core zones are characterized by foliated fault rocks cut by sharp fault planes

141 (Fig. 3a-d). Breccia lenses are developed in the Buron thrust core (Fig. 4d). Calcite mineralizations

142 in extensional veins (Buron, Arguel, Montlebon, Vue des Alpes, and Pratz) and in [slickenfibers](#)

143 (Fuans, Vue des Alpes, and Pratz) were sampled.

144 Extensional veins occur in limestone fragments of foliated fault rocks (Fig. 3e,g) and in clasts

145 from breccias (Figs. 3f and 4g). In limestone fragments of foliated fault rocks, extensional veins are

146 oriented perpendicularly to stylolites (Fig. 3e,g), which occur along S- and C-planes. Extensional

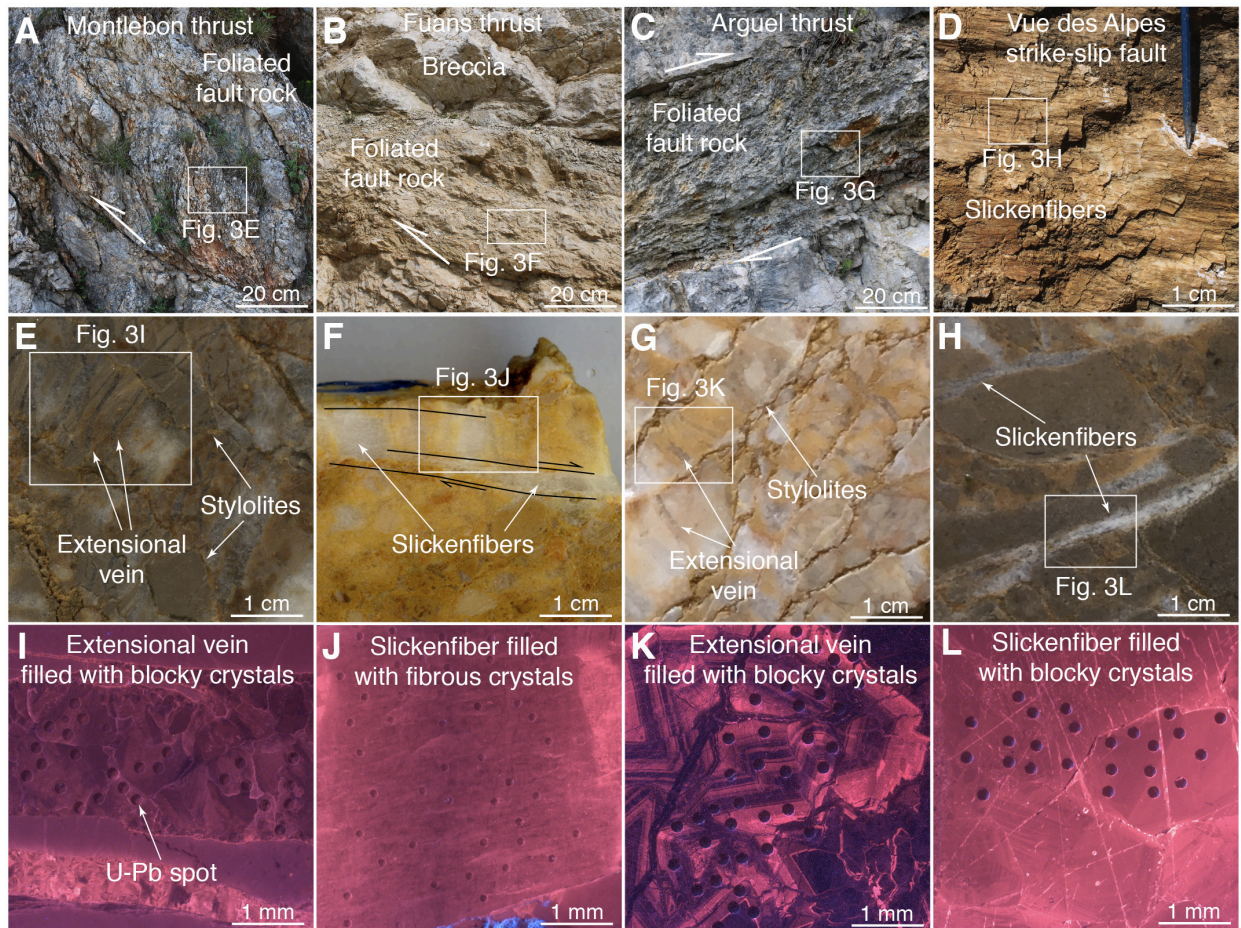
147 veins in clasts from breccias show a crackle-like texture and mutually cross-cutting relationships

148 (Fig. 3f). Extensional veins are filled by blocky to elongated-blocky calcite crystals and show

149 syntaxial growth (Figs. 3i-k, 4g, S1a-d, S2a,b,g,h, S3a-h).

150 The fault planes are coated by slickenfibers (Figs. 3d,h and 4e,f). At the microscale,  
 151 slickenfibers occur in dilational jogs along shear planes (Fig. 3h) and are filled by fibrous calcite  
 152 crystals bounded by sharp shear planes (Figs. 3j, 4i, S1e-h, and S2c-f) and/or by blocky calcite  
 153 crystals (Figs. 3l and 4h). Fibrous crystals are oriented parallel to shear planes.

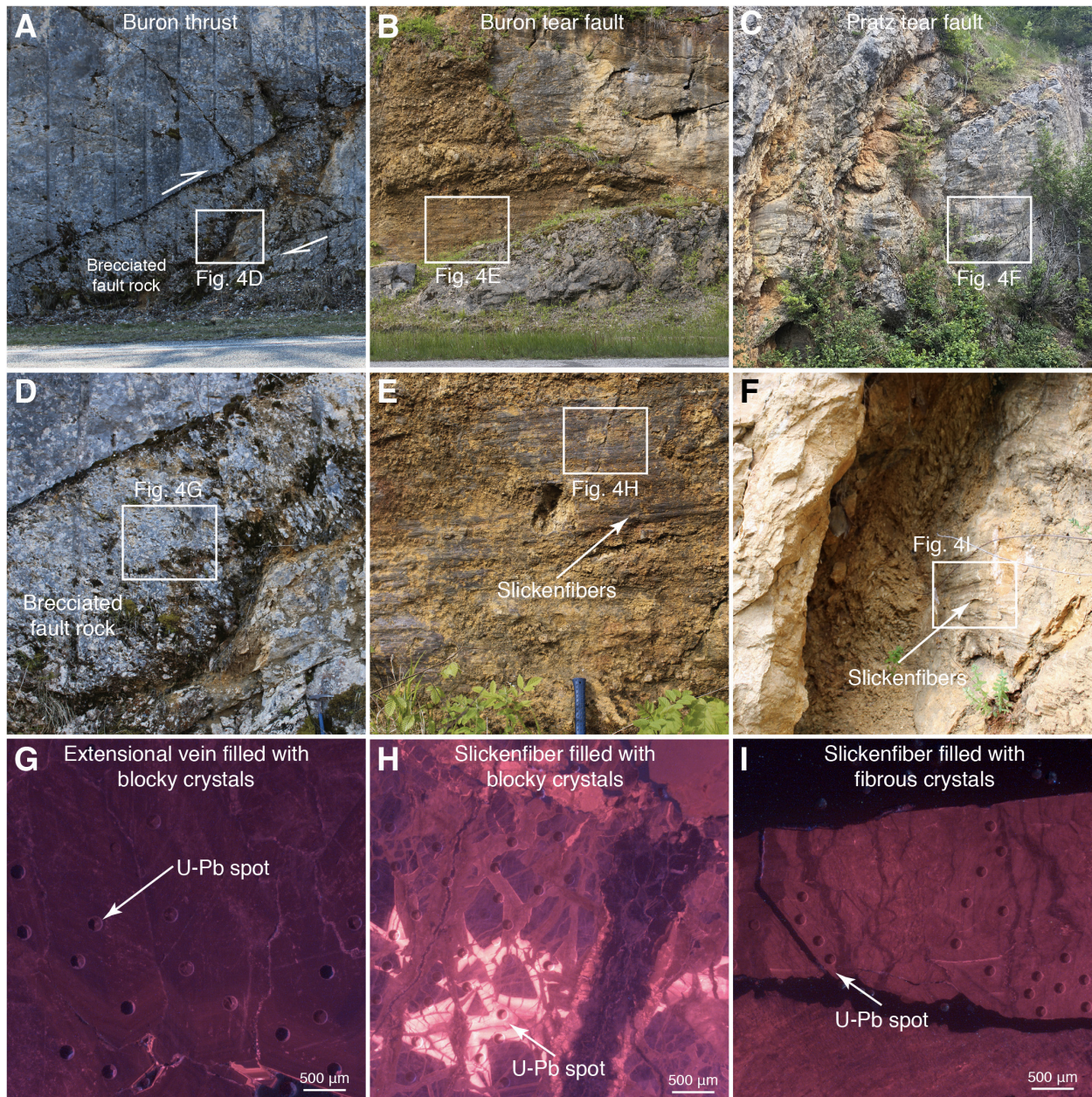
154 Most of the studied veins and slickenfibers show homogeneous cathodoluminescence colors,  
 155 ranging from bright to dull red, and/or show cathodoluminescence zoning on the same crystal (Figs.  
 156 3i-l, 4g-i, S1a,c,e,g, S2a,c,e,g, and S3a,c,e,g). In places, slickenfibers and extensional veins are  
 157 cross-cut by extensional veins showing black to dull red luminescence colors (Figs. S1e-h, S2c-f,  
 158 and S3a,b,g,h)



159  
 160 **Figure 3.** Foliated fault rocks in the fault core of the Montlebon thrust (a), Arguel thrust (b), and (c) Fuans thrust. (d)  
 161 Detail of minor fault plane along the Vue des Alpes strike-slip fault showing calcite slickenfibers. (e) Hand sample from  
 162 the Montlebon thrust showing host rock sigmoids bounded by stylolites and extensional veins perpendicular to  
 163 stylolites. (f) Hand sample from the Fuans thrust showing host rock sigmoids bounded by stylolites and extensional



164 veins perpendicular to stylolites. **(g)** Hand sample from the [Arguel](#) thrust showing extensional veins with crackle-like  
 165 texture. **(h)** Hand sample from a minor fault plane along the Vue des Alpes strike-slip fault showing [slickenfibers](#)  
 166 developed along dissolution planes. **(i-l)** Cathodoluminescence microphotographs of thin sections showing extensional  
 167 [veins](#) and [slickenfibers](#) from the studied faults with ablation craters of the U-Pb analyses.  
 168



169  
 170 **Figure 4.** **(a)** Buron thrust. **(b)** Buron tear fault. **(c)** Pratz tear fault. **(d)** Brecciated fault rocks in the fault core of the  
 171 Buron thrust. **(e)** Brecciated fault rocks cut by sharp fault planes in the fault core of the Buron tear fault. **(f)** Foliated  
 172 fault rock cut by sharp fault planes in the fault core of the Pratz tear fault. **(g-i)** Cathodoluminescence microphotographs

173 of thin sections showing extensional veins and slickenfibers from the studied faults with ablation craters of the U-Pb  
174 analyses.

175

#### 176 4. 2 U-Pb dating

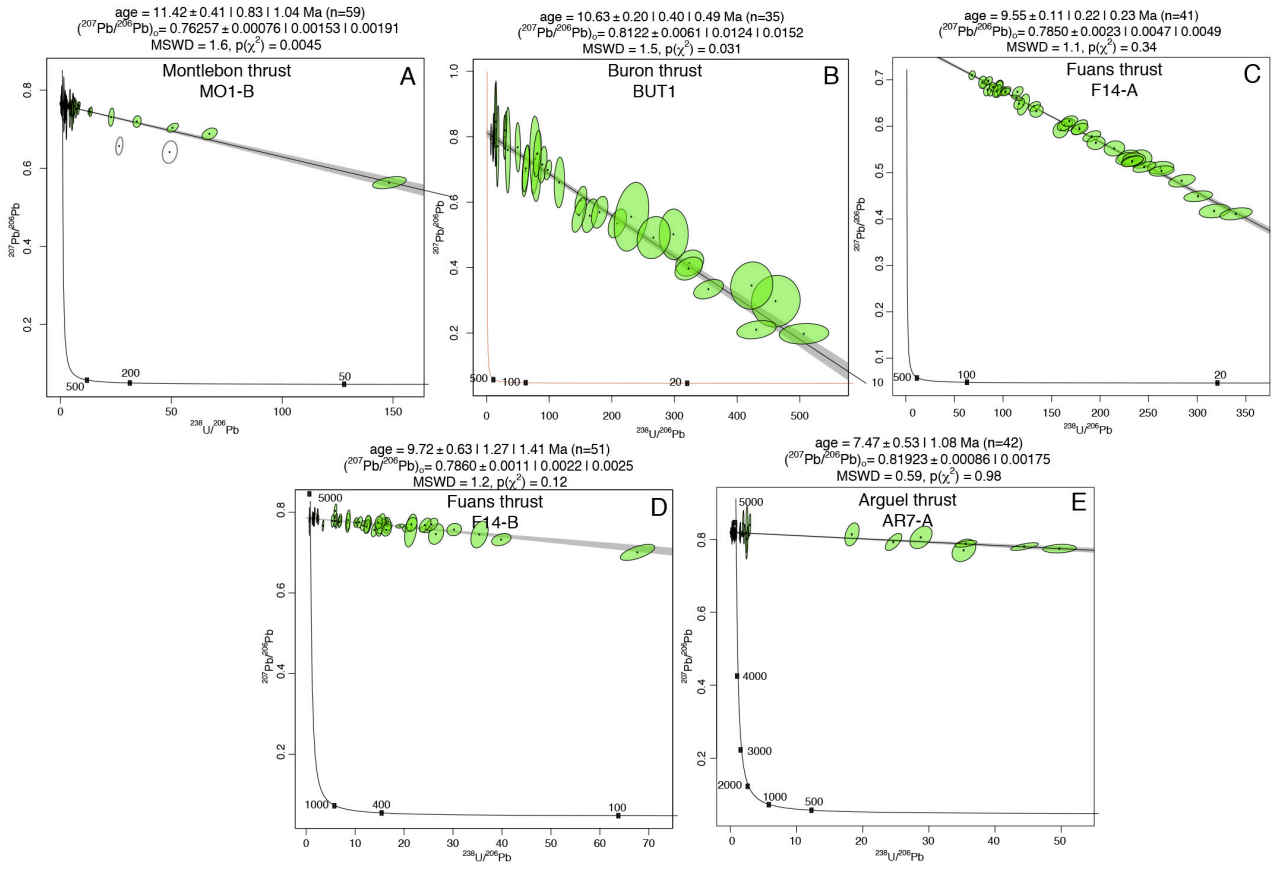
177 A total of 12 reliable lower intercept ages (Figs. 5 and 6) out of 19 analyses (rejected age data  
178 is presented in Fig. S4) are reported with uncertainties at  $2\sigma$  absolute including counting statistics  
179 uncertainties, uncertainty of the primary reference material and inter-session variations (Guillong et  
180 al., 2020). The U-Pb ages indicate different phases of tectonic activity and related calcite  
181 precipitation in the middle Eocene to Pliocene period and also multiple precipitation ages along the  
182 same fault (Supplementary Information Table 1).

183 An extensional vein from the Montlebon thrust shows a Serravallian age of  $11.4 \pm 1.1$  Ma  
184 (Fig. 5a). An extensional vein from the Buron thrust shows a Tortonian age of  $10.6 \pm 0.5$  Ma (Fig.  
185 5b). Two slickenfibers from the Fuans thrust yield Tortonian ages indistinguishable from each other  
186 of  $9.7 \pm 1.4$  Ma and  $9.6 \pm 0.3$ , respectively (Fig. 5c,d). An extensional vein from the Arguel thrust  
187 shows a Tortonian-Messinian age of  $7.5 \pm 1.1$  Ma (Fig. 5e). Along the Vue des Alpes strike-slip  
188 fault, two slickenfibers yield Ypresian-Lutetian ages of  $44.7 \pm 2.6$  and  $48.4 \pm 1.5$  Ma (Fig. 6a,b),  
189 while an extensional vein shows a Pliocene age of  $3.9 \pm 2.9$  Ma (Fig. 6c). An extensional vein from  
190 the Buron strike-slip fault shows a Messinian age of  $5.7 \pm 4.7$  Ma (Fig. 6d). One slickenfiber and  
191 one extensional vein from the Pratz strike-slip fault show Tortonian-Messinian ages of  $10.5 \pm 0.4$   
192 and  $9.1 \pm 6.5$  Ma (Fig. 6f-g), while one slickenfiber shows a younger age of  $4.8 \pm 1.7$  Ma (Fig. 6e).  
193 Because of the common-lead rich  $^{207}\text{Pb}/^{206}\text{Pb}$  compositions, the U-Pb ages of the samples DA2,  
194 BUS1, PR1-A, PR2-2 of the strike-slip faults have larger uncertainties than those of the thrusts.

195

196

## U-Pb ages from thrusts



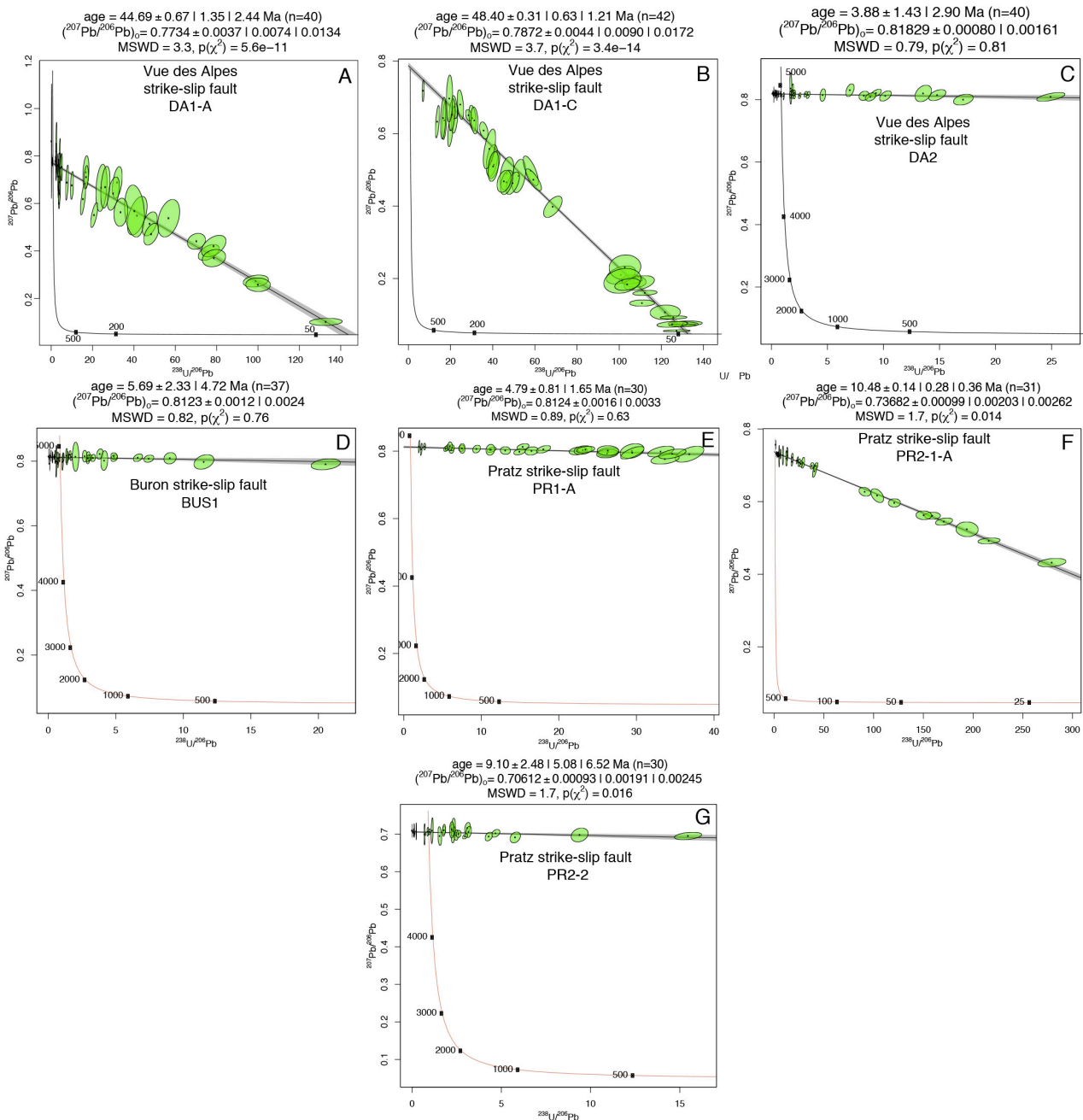
197

198

199

**Figure 5.** Tera-Wasserburg concordia diagrams of thrust faults. **(a)** Montlebon thrust. **(a)** Buron thrust. **(c,d)** Fuans thrust. **(e)** Arguel thrust.

## U-Pb ages from strike-slip faults



201

202 [Figure 6. Tera-Wasserburg concordia diagrams of strike-slip faults. \(a-c\) Vue des Alpes strike-slip fault. \(d\) Buron](#)  
 203 [strike-slip fault. \(e-g\) Pratz strike-slip fault.](#)

204

205

## 5. Discussion and conclusions

206 Slickenfibers on sharp fault planes are clear evidence of tectonic slip along faults (Figs. 3j-l,  
207 4i, S1e-h, and S2c,f). In particular, blocky and fibrous crystals indicate respectively fast and slow  
208 vein opening rates associated with fault slip. Within slickenfibers, calcite crystal precipitated during  
209 syn- to early post-slip fluid influx in newly formed dilational sites formed along undulated and  
210 sharp slip planes (Gratier and Gamond, 1990; Urai et al., 1991; Holland and Urai, 2010; Fagereng et  
211 al., 2010; Bons et al., 2012; Woodcock et al., 2014). Extensional veins oriented perpendicular to  
212 stylolites (Fig. 3e,g) are linked to syn-thrusting shortening (Gratier et al., 2013). The studied veins  
213 are therefore interpreted as the product of tectonic fault slip and their U-Pb ages are considered as  
214 representative of faulting activity.

215 We recognize three regional tectonic phases between the middle Eocene and the Pliocene  
216 (Figs. 7 and 8) which are linked to the long-lived tectonic activity of the Alpine foreland evolution.  
217 The presented ages should be regarded as minimum ages for the onset of deformation at the studied  
218 faults or as maximum ages for its termination as potentially older or younger deformation phases  
219 recorded by other veins and slickenfibers not sampled and analyzed here may have been missed.

220 The U-Pb ages are regionally consistent in terms of tectonic evolution of the Jura FTB and the  
221 microstructures of the analyzed veins and slickenfibers indicate precipitation during syn- to early  
222 post-slip fluid influx. However, although U-Pb dating was performed on crystals with no indication  
223 of later open-system alteration based on CL-microscopy, possible late fluid infiltration and calcite  
224 recrystallization cannot be excluded as previously suggested by other studies (Beaudoin et al., 2018;  
225 Hoareau et al., 2021; Roberts et al., 2020, 2021).

226 Sample BUS1 clearly shows multiple calcite phases indicating vein re-opening and  
227 potentially different ages (Fig. 4h). However, the Tera-Wasserburg diagram of BUS1 shows a  
228 single age trend with a low MSWD of 0.82 (Fig. 6d). This would not be observed in a sample that  
229 experienced crystallization at significantly different times. Therefore, sample BUS1 reflects calcite  
230 precipitation within a time interval smaller than what would result in multiple age trends.

231 The oldest tectonic phase is recorded by two horizontal [slickenfibers](#) dated at  $44.7 \pm 2.6$  and  
232  $48.4 \pm 1.5$  Ma in Ypresian-Lutetian times (middle Eocene) along the Vue des Alpes strike-slip fault  
233 ([Fig. 7](#)). These ages are  $\sim 10$  Ma older than the onset of the extensional tectonic activity in  
234 Priabonian (late Eocene) related to Rhine Graben opening ([Sissingh, 1998](#); [Mazurek et al. 2018](#)).  
235 The strike-slip faulting in Eocene times is consistent with fault-slip data of [Homberg et al. \(1997\)](#).  
236 [We propose that the Ypresian-Lutetian tectonic activity can be related to the late Mesozoic-Eocene](#)  
237 [far field tectonic shortening in the European plate foreland due to the advancing Alpine orogen](#)  
238 [\(Mazurek et al., 2006; Timar-Geng et al., 2006\) \(Fig. 8a\). On the contrary, previous studies](#)  
239 [suggested that middle Eocene strike-slip faulting in the Jura area was related to the far-field effect](#)  
240 [of the Pyrenean compression \(Bergerat, 1987; Homberg et al., 2002\). The Pyrenean far field effect](#)  
241 [has also been recognized in the Paris Basin \(eg, Lacombe et al., 1990; Lacombe and Mouthereau,](#)  
242 [1999; Lacombe and Obert, 2000\), in eastern France \(Lacombe et al., 1993\), and even in the UK](#)  
243 [\(Hibsch et al., 1995\) where Pyrenean-related calcite veins were dated by U-Pb \(Parrish et al., 2018\).](#)  
244 [However, even though tectonic stresses have been shown to be transmitted more than thousand km](#)  
245 [away from the orogenic front \(Craddock et al., 1993; Beaudoin and Lacombe, 2018\), further studies](#)  
246 [are necessary to better constrain the origin of pre-Miocene fault activity in the European foreland.](#)  
247 [Structural analyses of the studied thrusts highlight N to NW oriented tectonic transport](#)  
248 [directions \(Fig. 4a-d\) consistent with the regional NW-SE to N-S compressional phase that has](#)  
249 [affected the Jura fold and thrust belt since the Miocene \(Philippe et al, 1996; Becker, 2000;](#)  
250 [Homberg et al., 2002; Ustaszewski and Schmid, 2006; Madritsch et al., 2008; Looser et al., 2021\).](#)  
251 Although age uncertainties do not allow a distinction beyond doubt and the limited numbers of U-  
252 Pb ages and studied thrusts provide a limited picture, the Jura imbrication seems to have occurred  
253 by in-sequence thrusting. The oldest observed thrusts ages are Serravallian-Messinian and become  
254 progressively younger moving from the inner (SE) toward the external (NW) part, from  $11.4 \pm 1.1$ ,  
255  $10.6 \pm 0.5$ ,  $9.7 \pm 1.4$  and  $9.6 \pm 0.3$  on the same thrust, and  $7.5 \pm 1.1$  Ma, respectively, in the  
256 Montlebon, Buron, Fuans, and Arguel thrusts ([Figs. 7 and 8b](#)). These ages are consistent with the

257 time interval of ~14.5-3.3 Ma suggested for thrusting activity from biostratigraphic dating of syn- to  
258 post-tectonic sediments (Becker, 2000 and references therein) and from calcite U-Pb ages of thrust  
259 activity in the eastern Jura FTB (Looser et al., 2021) (Fig. 7).

260 Previous studies interpreted the subvertical strike-slip faults in the Jura FTB as tear faults,  
261 with activity during thrusting and folding (Sommaruga, 1997; Looser et al., 2021). Our structural  
262 analyses and U-Pb ages from the studied strike-slip faults support this interpretation. In particular,  
263 strike-slip faults are subvertical and are roughly parallel or oblique to the regional transport  
264 directions inferred from thrust kinematics (compare tectonic transport directions of Fig. 4a-d with  
265 those of Fig. 4f,g), a common feature of tear faults (Twiss and Moores, 1992).

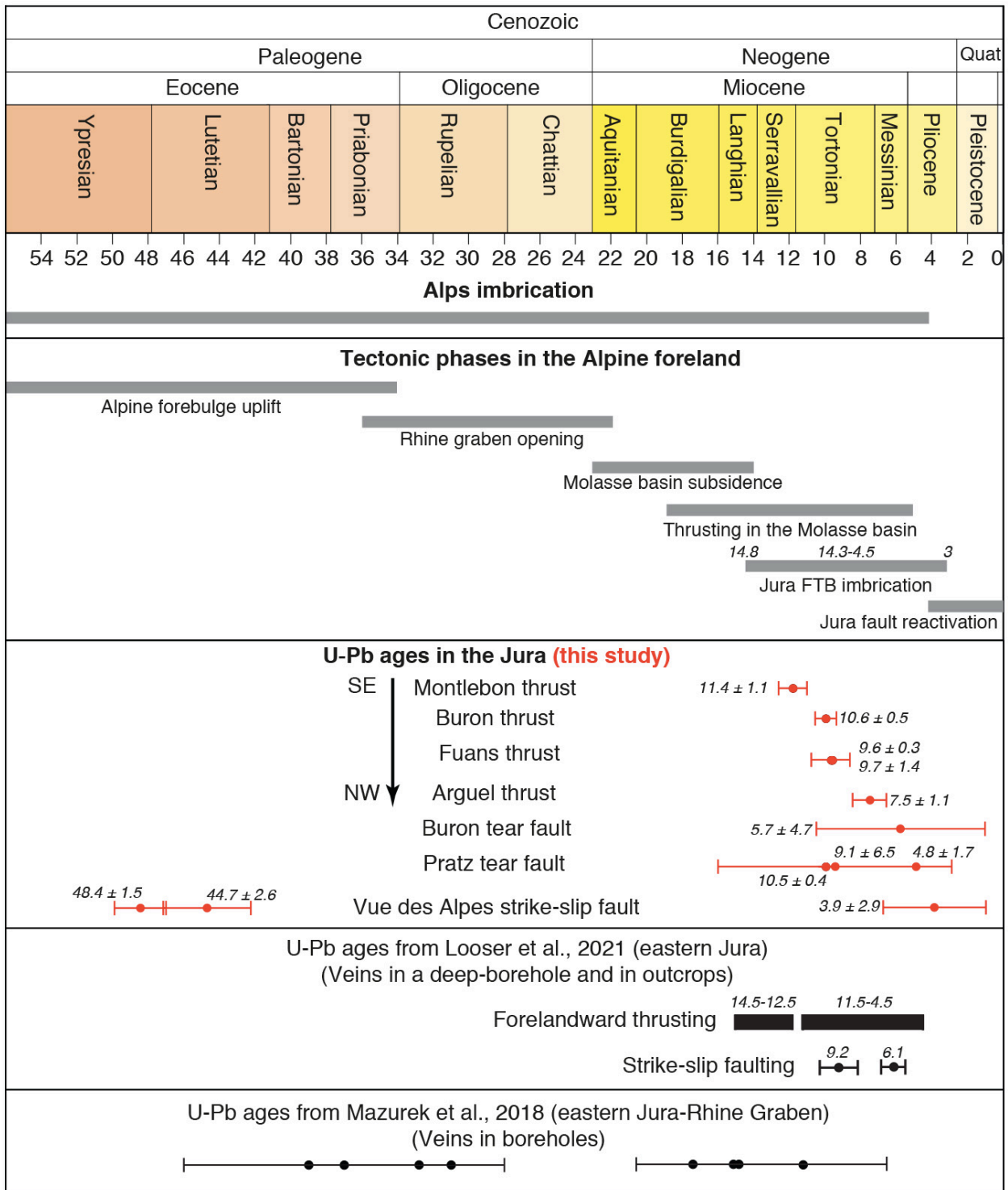
266 The Buron thrust, active at  $10.6 \pm 0.5$  Ma, was cross-cut by the Buron tear fault ~5 Ma later,  
267 at  $5.7 \pm 4.7$  Ma (Figs. 7 and 8c). The Pratz tear fault was active at  $10.5 \pm 0.4$  and  $9.1 \pm 6.5$  Ma,  
268 indicating tear faulting generation during coeval thrust propagation, and further late-orogenic re-  
269 activation at  $4.8 \pm 1.7$  Ma (Figs. 7 and 8b). These data indicate that tear faulting occurred during  
270 syn- to late-orogenic times (Fig. 8b,c). In addition, a late-orogenic phase is recorded by an  
271 extensional vein from the Vue des Alpes strike-slip fault showing a Pliocene age of  $3.9 \pm 2.9$  Ma  
272 (Fig. 7). This age has been measured on an extensional vein that cannot be directly related to fault  
273 slip. Therefore, we cannot completely exclude that this age represents a late alteration event not  
274 directly linked to fault slip during the Pliocene. However, the  $3.9 \pm 2.9$  Ma age is consistent with  
275 late orogenic deformation between 4.2 and 2.9 Ma documented in the frontal part of the Jura FTB  
276 (Madritsch et al., 2008 and references therein). The  $3.9 \pm 2.9$  Ma age from the Vue des Alpes strike-  
277 slip fault is ~40 Ma younger than the middle Eocene ages ( $44.7 \pm 2.6$  and  $48.4 \pm 1.5$  Ma) measured  
278 on the same fault, suggesting the reactivation of the Vue des Alpes strike-slip fault during late Jura  
279 shortening. This inference is also consistent with field cross-cutting relationships indicating re-  
280 activation of pre-existing strike-slip faults as tear faults (Homberg et al., 1997).

281 We consider the retrieved age as fault re-activation of the Vue des Alpes strike-slip fault and  
282 relate it to a stress change from pure compression to strike-slip state of stress coupled with the

283 occurrence of an inherited strike-slip fault favorably oriented with respect to the regional stress  
284 field. This stress change associated with tear fault development can be related to progressive fold-  
285 and-thrust belt thickening and erosion initiating only after ~4.5 Ma (Looser et al., 2021 and  
286 references therein), which led to an increase in the maximum vertical stress ( $\sigma_3$ ) and a switch  
287 between  $\sigma_3$  and 2 (Ferril et al., 2021). Shortening is still active in the Jura FTB and tear faults  
288 (also re-activated tear faults) are seismogenic (Thouvenot et al., 1998).

289         The presented tectonic reconstruction depicts a stable evolution of the Jura FTB wedge by  
290 possible in-sequence thrusting consistent with thrust imbrication above the low-friction décollement  
291 consisting of evaporites (Fig. 8a-c). Contrarily, out-of-sequence thrusting occurred as late as in  
292 Messinian-early Pliocene times in the proximal Molasse Basin (Von Hagke et al., 2012, 2014) and  
293 in the Alps (Bellahsen et al., 2014). This tectonic framework suggests a stable topographic  
294 evolution of the critical taper and topographic profile of the Jura fold-and-thrust belt. Finally, this  
295 study constrains a long-lived polyphase tectonic history of the northwestern Alpine foreland system  
296 along the convergent boundary between European and African plates from the middle Eocene to the  
297 Pliocene.





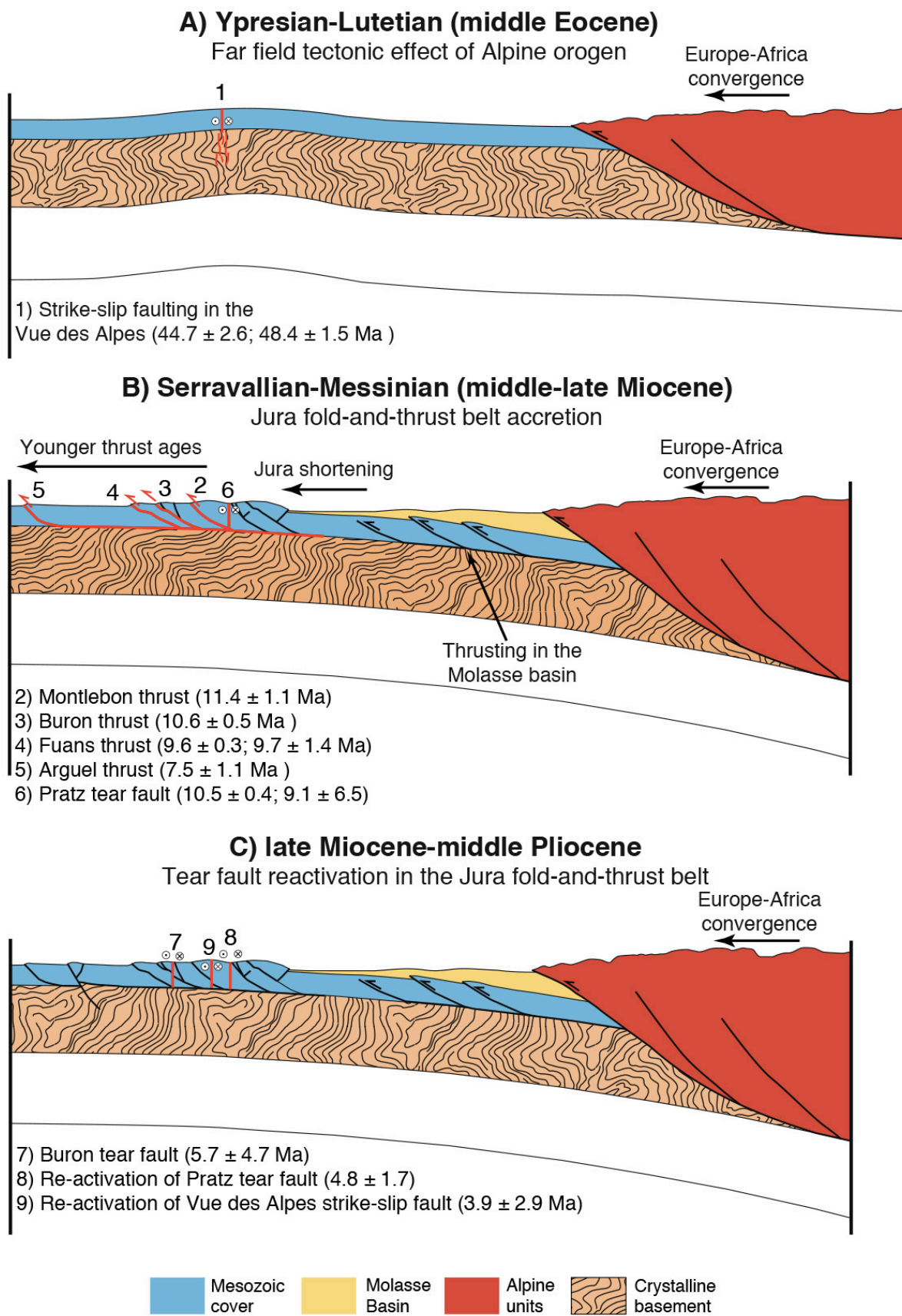
298

299

300

301

**Figure 7.** Main tectonic phases in the Alps and in the Alpine foreland. Age constraints shown as grey bars are from Burkhard and Sommaruga (1998), Ustaszewski et al. (2006), Madritsch et al. (2008), Bellahsen et al. (2014), and Von Hagke et al. (2014). For calcite U-Pb data, all uncertainties are represented as  $2\sigma$ .



302

303

304

**Figure 8.** (a-d) Schematic reconstruction of the main tectonic phases dated in the Jura area in the regional context of the Alpine foreland system evolution.

305

## 306 ACKNOWLEDGEMENT

307 We thank CASP (<https://www.casp.org.uk/>) for financial support during fieldwork activity by  
308 the Andy Whitham Fieldwork Award 2019 to L. Smeraglia. Financial support by Borsa di  
309 Perfezionamento Estero 2017 (Sapienza) to L. Smeraglia, UMR 6249 and OSU Theta projects to O.  
310 Fabbri and F. Choulet are acknowledged. U-Pb analyses were funded by the Swiss National Science  
311 Foundation project number 200021\_169849 to S. M. Bernasconi. We thank J. Mosar, M. Schori, A.  
312 Sommaruga, C. Mottran, L. Weiss, and C. Von Hagke for constructive discussions and suggestions,  
313 also during fieldwork. We thank the Editor Susanne Buiter and two Reviewers Olivier Lacombe  
314 and Nick Roberts for their constructive comments that helped to improve the manuscript.

315

## 316 REFERENCES

- 317 [Affolter, T., and Gratier, J. P.: Map view retrodeformation of an arcuate fold-and-thrust belt: The](#)  
318 [Jura case. \*Journal of Geophysical Research: Solid Earth\*, 109\(B3\), 2004.](#)
- 319 [Beaudoin, N., and Lacombe, O.: Recent and future trends in paleopiezometry in the diagenetic](#)  
320 [domain: Insights into the tectonic paleostress and burial depth history of fold-and-thrust belts](#)  
321 [and sedimentary basins. \*Journal of Structural Geology\*, 114, 357-365, 2018.](#)
- 322 [Beaudoin, N., Leprêtre, R., Bellahsen, N., Lacombe, O., Amrouch, K., Callot, J. P., ... and Daniel, J.](#)  
323 [M.: Structural and microstructural evolution of the Rattlesnake Mountain Anticline](#)  
324 [\(Wyoming, USA\): new insights into the Sevier and Laramide orogenic stress build-up in the](#)  
325 [Bighorn Basin. \*Tectonophysics\*, 576, 20-45, 2012.](#)
- 326 Beaudoin, N., Lacombe, O., Roberts, N. M., and Koehn, D.: U-Pb dating of calcite veins reveals  
327 complex stress evolution and thrust sequence in the Bighorn Basin, Wyoming, USA.  
328 *Geology*, 46(11), 1015-1018, 2018.
- 329 Becker, A.: The Jura Mountains - an active foreland fold-and-thrust belt?. *Tectonophysics*, 321(4),  
330 381-406, 2000.

- 331 Bellahsen, N., Mouthereau, F., Boutoux, A., Bellanger, M., Lacombe, O., Jolivet, L., and Rolland,  
332 Y. : Collision kinematics in the western external Alps. *Tectonics*, 33(6), 1055-1088, 2014.
- 333 Bergerat, F.: Stress fields in the European platform at the time of Africa-Eurasia collision.  
334 *Tectonics* 6, 99-132, 1987.
- 335 [Bons, P. D., Elburg, M. A., and Gomez-Rivas, E.: A review of the formation of tectonic veins and](#)  
336 [their microstructures. \*Journal of Structural Geology\*, 43, 33-62, 2012.](#)
- 337 Carminati E., Aldega L., Smeraglia L., Scharf A., Mattern F., Albert R., and Gerdes A.: Tectonic  
338 evolution of the Northern Oman Mountains, part of the Straits of Hormuz Syntaxis: new  
339 structural and paleothermal analyses and U-Pb dating of synkinematic calcite. *Tectonics* 39,  
340 e2019TC005936, 2020.
- 341 Craig, M. S., and Warvakai, K.: Structure of an active foreland fold and thrust belt, Papua New  
342 Guinea. *Australian Journal of Earth Sciences*, 56(5), 719-738, 2009.
- 343 [Craddock, J. P., Jackson, M., van der Pluijm, B. A., & Versical, R. T.: Regional shortening fabrics](#)  
344 [in eastern North America: Far-field stress transmission from the Appalachian-Ouachita](#)  
345 [Orogenic Belt. \*Tectonics\*, 12\(1\), 257-264, 1993.](#)
- 346 Fagereng, Å., Remitti, F., and Sibson, R. H.: Shear veins observed within anisotropic fabric at high  
347 angles to the maximum compressive stress. *Nature Geoscience*, 3(7), 482, 2010.
- 348 [Ferril, D.A., Smart, K.J., Cawood, A.J., Morris, A.P.: The fold-thrust belt stress cycle:](#)  
349 [Superposition of normal, strike-slip, and thrust faulting deformation regimes. \*Journal of\*](#)  
350 [Structural Geology](#) 148, 104362, 2021.
- 351 Goodfellow, B. W., Viola, G., Bingen, B., Nuriel, P., and Kylander-Clark, A. R.: Paleocene faulting  
352 in SE Sweden from U–Pb dating of slickenfiber calcite. *Terra Nova*, 29(5), 321-328, 2017.
- 353 Gratier, J. P., and Gamond, J. F.: Transition between seismic and aseismic deformation in the upper  
354 crust. Geological Society, London, Special Publications, 54(1), 461-473, 1990.

355 Gratier, J.P., Thouvenot, F., Jenatton, L., Tourette, A., Doan, M.L., Renard, F.: Geological control  
356 of the partitioning between seismic and aseismic sliding behaviours in active faults: evidence  
357 from the Western Alps, France. *Tectonophysics* 600, 226-242, 2013.

358 [Gruber, M.: Structural Investigations of the Western Swiss Molasse Basin - From 2D Seismic  
359 Interpretation to a 3D Geological Model. \*GeoFocus\*, 41, 190 pp, 2017.](#)

360 [Guillong, M., Wotzlaw, J., Looser, N., & Laurent, O. \(2020\). Evaluating the reliability of U–Pb  
361 laser ablation inductively coupled plasma mass spectrometry \(LA-ICP-MS\) carbonate  
362 geochronology: Matrix issues and a potential calcite validation reference material.  
363 \*Geochronology\*, 2, 155–167. <https://doi.org/10.5194/gchron-2-155-2020>.](#)

364 Hansman, R. J., Albert, R., Gerdes, A., and Ring, U.: Absolute ages of multiple generations of  
365 brittle structures by U-Pb dating of calcite. *Geology*, 46(3), 207-210, 2018.

366 [Hibsch, C., Jarrige, J. J., Cushing, E. M., and Mercier, J.: Palaeostress analysis, a contribution to the  
367 understanding of basin tectonics and geodynamic evolution. Example of the  
368 Permian/Cenozoic tectonics of Great Britain and geodynamic implications in western Europe.  
369 \*Tectonophysics\*, 252\(1-4\), 103-136, 1995.](#)

370 [Hoareau, G., Crognier, N., Lacroix, B., Aubourg, C., Roberts, N. M., Niemi, N., ... and Ruiz, I. S.:  
371 Combination of  \$\Delta 47\$  and U-Pb dating in tectonic calcite veins unravel the last pulses related to  
372 the Pyrenean Shortening \(Spain\). \*Earth and Planetary Science Letters\*, 553, 116636, 2021.](#)

373 [Holland, M., and Urai, J. L.: Evolution of anastomosing crack–seal vein networks in limestones:  
374 Insight from an exhumed high-pressure cell, Jabal Shams, Oman Mountains. \*Journal of  
375 Structural Geology\*, 32\(9\), 1279-1290, 2010.](#)

376 Homberg, C., Hu, J. C., Angelier, J., Bergerat, F., and Lacombe, O.: Characterization of stress  
377 perturbations near major fault zones: insights from 2-D distinct-element numerical modelling  
378 and field studies (Jura mountains). *Journal of Structural Geology*, 19(5), 703-718, 1997.

379 Homberg, C., Bergerat, F., Philippe, Y., Lacombe, O., and Angelier, J.: Structural inheritance and  
380 Cenozoic stress fields in the Jura fold-and-thrust belt (France). *Tectonophysics*, 357(1-4),  
381 137-158, 2002.

382 [Jordan, P.: Evidence for large-scale decoupling in the Triassic evaporites of Northern Switzerland:  
383 an overview. \*Eclogae Geologicae Helvetiae\*, 85, 677–693, 1992.](#)

384 [Lacombe, O., Angelier, J., Laurent, P., Bergerat, F., and Tournier, C.: Joint analyses of calcite  
385 twins and fault slips as a key for deciphering polyphase tectonics: Burgundy as a case study.  
386 \*Tectonophysics\*, 182\(3-4\), 279-300, 1990.](#)

387 [Lacombe, O., Angelier, J., Byrne, D., and Dupin, J. M.: Eocene-Oligocene tectonics and kinematics  
388 of the Rhine-Saone continental transform zone \(eastern France\). \*Tectonics\*, 12\(4\), 874-888,  
389 1993.](#)

390 [Lacombe, O., and Mouthereau, F.: What is the real front of orogens? The Pyrenean orogen as a case  
391 study. \*Comptes Rendus de l'Academie des Sciences Series IIA Earth and Planetary Science\*,  
392 329\(12\), 889-896, 1999.](#)

393 [Lacombe, O., & Mouthereau, F. \(2002\). Basement-involved shortening and deep detachment  
394 tectonics in forelands of orogens: Insights from recent collision belts \(Taiwan, Western Alps,  
395 Pyrenees\). \*Tectonics\*, 21\(4\), 12-1.](#)

396 [Lacombe, O., and Obert, D.: Structural inheritance and cover deformation: Tertiary folding and  
397 faulting in, the western Paris Basin. \*Comptes rendus de l'academie des sciences serie ii  
398 fascicule a-sciences de la terre et des planetes\*, 330\(11\), 793-798, 2000.](#)

399 Lacombe, O., Lavé, J., Roure, F. M., and Vergés, J. (Eds.): Thrust belts and foreland basins: From  
400 fold kinematics to hydrocarbon systems. Springer Science & Business Media, 2007.

401 [Lacombe, O., and Bellahsen, N.: Thick-skinned tectonics and basement-involved fold–thrust belts:  
402 insights from selected Cenozoic orogens. \*Geological Magazine\*, 153, 763-810, 2016.](#)

403 [Looser, N., Madritsch, H., Guillong, M., Laurent, O., Wohlwend, S., & Bernasconi, S. M. \(2021\).  
404 Absolute age and temperature constraints on deformation along the basal décollement of the](#)

405 [Jura fold-and- thrust belt from carbonate U-Pb dating and clumped isotopes. \*Tectonics\*, 40,](#)  
406 [e2020TC006439. <https://doi.org/10.1029/2020TC006439>](#)

407 Madritsch, H., Schmid, S. M., and Fabbri, O.: Interactions between thin- and thick-skinned tectonics  
408 at the northwestern front of the Jura fold-and-thrust belt (eastern France). *Tectonics*, 27, 1-31,  
409 2008.

410 Mazurek, M., Davis, D. W., Madritsch, H., Rufer, D., Villa, I. et al. (2018). Veins in clay-rich  
411 aquitards as records of deformation and fluid-flow events in northern Switzerland. *Applied*  
412 *Geochemistry*, 95, 57-70, 2008.

413 Mazurek, M., Hurford, A. J., and Leu, W.: Unravelling the multi-stage burial history of the Swiss  
414 Molasse Basin: integration of apatite fission track, vitrinite reflectance and biomarker  
415 isomerisation analysis. *Basin Research*, 18, 27–50, 2006.

416 [Mosar, J.: Present-day and future tectonic underplating in the western Swiss Alps: reconciliation of](#)  
417 [basement/wrench-faulting and décollement folding of the Jura and Molasse basin in the](#)  
418 [Alpine foreland. \*Earth and Planetary Science Letters\*, 173, 143-155, 1999.](#)

419 Nuriel, P., Weinberger, R., Kylander-Clark, A. R. C., Hacker, B. R., and Craddock, J. P.: The onset  
420 of the Dead Sea transform based on calcite age-strain analyses. *Geology*, 45(7), 587-590,  
421 2017.

422 [Parrish, R. R., Parrish, C. M., and Lasalle, S.: Vein calcite dating reveals Pyrenean orogen as cause](#)  
423 [of Paleogene deformation in southern England. \*Journal of the Geological Society\*, 175\(3\),](#)  
424 [425-442, 2018.](#)

425 [Philippe, Y., Colletta, B., Deville, E., and Mascle, A.: The Jura fold-and-thrust belt: a kinematic](#)  
426 [model based on map-balancing. \*Mémoires du Muséum national d'histoire naturelle\*, 170, 235-](#)  
427 [261, 1996.](#)

428 [Pfiffner, O. A.: \*Geology of the Alps\*. Chichester: John Wiley & Son, 2014.](#)

429 Rime, V., Sommaruga, A., Schori, M., and Mosar, J. : Tectonics of the Neuchâtel Jura Mountains:  
430 insights from mapping and forward modelling. *Swiss Journal of Geosciences*, 112, 563-578,  
431 2019.

432 Roberts, N. M., Drost, K., Horstwood, M. S., Condon, D. J., Chew, D., Drake, H., and Haslam, R.:  
433 Laser ablation inductively coupled plasma mass spectrometry (LA-ICP-MS) U-Pb carbonate  
434 geochronology: strategies, progress, and limitations. *Geochronology*, 2(1), 33-61, 2020.

435 [Roberts, N. M., Žák, J., Vacek, F., and Sláma, J.: No more blind dates with calcite: Fluid-flow vs.](#)  
436 [fault-slip along the Očkov thrust, Prague Basin. \*Geoscience Frontiers\*, 12\(4\), 101143, 2021.](#)

437 Sissingh, W.: Comparative Tertiary stratigraphy of the Rhine Graben, Bresse Graben and Molasse  
438 Basin: correlation of Alpine foreland events. *Tectonophysics*, 300, 249–28, 1998.

439 Smeraglia, L., Aldega, L., Billi, A., Carminati, E., Di Fiore, F., Gerdes, A., and Vignaroli, G.:  
440 Development of an Intrawedge Tectonic Mélange by Out-of-Sequence Thrusting, Buttressing,  
441 and Intraformational Rheological Contrast, Mt. Massico Ridge, Apennines, Italy. *Tectonics*,  
442 38(4), 1223-1249, 2019.

443 Smeraglia, L., Fabbri, O., Choulet, F., Buatier, M., Boulvais, P., Bernasconi, S.M., and Castorina,  
444 F.: Syntectonic fluid flow and deformation mechanisms within the frontal thrust of foreland  
445 fold-and-thrust belt: Example from the Internal Jura, Eastern France. *Tectonophysics*, 778,  
446 <https://doi.org/10.1016/j.tecto.2019.228178>, 2020.

447 Sommaruga, A.: Geology of the Central Jura and the Molasse basin: New insight into an evaporite-  
448 based foreland fold and thrust belt. *Mémoires de la Société Neuchâteloise de Sciences*  
449 *Naturelles*, 12, pp. 176, 1997.

450 [Sommaruga, A., Mosar, J., Schori, M., and Gruber, M.: The role of the Triassic evaporites](#)  
451 [underneath the North Alpine foreland. In Soto, J., Flinch, J., and Tari, G., \(Ed.\), \*Permo-\*](#)  
452 [Triassic salt provinces of Europe, North Africa and the Atlantic Margins: tectonics and](#)  
453 [hydrocarbon potential, chapter 22 \(IV\). Elsevier, 2017.](#)



- 454 Thouvenot, F., Fréchet, J., Tapponnier, P., Thomas, J. C., Le Brun, B., Ménard, G., and Paul, A.:  
455 The ML 5.3 Epagny (French Alps) earthquake of 1996 July 15: a long-awaited event on the  
456 Vuache Fault. *Geophysical Journal International*, 135(3), 876-892, 1998.
- 457 Timar-Geng, Z., Fu"genschuh, B., Wetzel, A., and Dresmann, H.: The low temperature thermal  
458 history of northern Switzerland as revealed by fission track analysis and inverse thermal  
459 modelling. *Eclogae Geologicae Helvetiae*, 99, 255–270, 2006.
- 460 [Twiss, R. J., and Moores, E. M.: Structural geology. Macmillan, 1992.](#)
- 461 [Urai, J. L., Williams, P. F., and Van Roermund, H. L. M.: Kinematics of crystal growth in  
462 syntectonic fibrous veins. \*Journal of Structural Geology\*, 13\(7\), 823-836, 1991.](#)
- 463 Ustaszewski, K., and Schmid, S. M.: Control of preexisting faults on geometry and kinematics in  
464 the northernmost part of the Jura fold-and-thrust belt. *Tectonics*, 25, 1-26, 2006.
- 465 Van der Pluijm, B. A., Hall, C. M., Vrolijk, P. J., Pevear, D. R., and Covey, M. C.: The dating of  
466 shallow faults in the Earth's crust. *Nature*, 412(6843), 172-175, 2001.
- 467 Vergés, J., Muñoz, J. A., and Martínez, A.: South Pyrenean fold and thrust belt: The role of foreland  
468 evaporitic levels in thrust geometry. In *Thrust tectonics*, 255-264. Springer, Dordrecht, 1992.
- 469 Von Hagke, C., Cederbom, C. E., Oncken, O., Stöckli, D. F., Rahn, M. K., and Schlunegger, F.:  
470 Linking the northern Alps with their foreland: The latest exhumation history resolved by low-  
471 temperature thermochronology. *Tectonics*, 31(5), 2012.
- 472 Von Hagke, C., Oncken, O., Ortner, H., Cederbom, C. E., and Aichholzer, S.: Late Miocene to  
473 present deformation and erosion of the Central Alps—Evidence for steady state mountain  
474 building from thermokinematic data. *Tectonophysics*, 632, 250-260, 2014.
- 475 Vrolijk, P., Pevear, D., Covey, M., and LaRiviere, A.: Fault gouge dating: history and evolution.  
476 *Clay Minerals*, 53(3), 305-324, 2018.
- 477 Woodcock, N. H., Miller, A. V. M., & Woodhouse, C. D.: Chaotic breccia zones on the Pembroke  
478 Peninsula, south Wales: Evidence for collapse into voids along dilational faults. *Journal of  
479 Structural Geology*, 69, 91-107, 2014.

